Bioresource Technology Reports 17 (2022) 100926

Contents lists available at ScienceDirect

Bioresource Technology Reports

journal homepage: www.sciencedirect.com/journal/bioresource-technology-reports

Pretreated residual biomasses in fluidized beds for chemical looping gasification: Analysis of devolatilization data by statistical tools

Andrea Di Giuliano [a], Marta Gallucci [b], Barbara Malsegna [a], Stefania Lucantonio [a], Katia Gallucci [a,*]

[a] Department of Industrial and Information Engineering and Economics (DIIIE), University of L'Aquila, Piazzale E. Pontieri 1-loc. Monteluco di Roio, 67100 L'Aquila, Italy

[b] Agenzia delle Entrate, via Giorgione n. 106, 00147 Rome, Italy

ARTICLE INFO

Keywords:
Linear regression
Oxygen carriers
Chemical looping gasification
Devolatilization
Torrefaction
Washing

ABSTRACT

Previously, this research group performed devolatilizations of different wheat straw pellets in fluidized beds, as a preliminary investigation for chemical looping gasification (European research project CLARA, G.A.817841). Performances were there evaluated by: (i) integral-average parameters (gas yield, carbon conversion, and H_2/CO molar ratio); (ii) syngas composition at the peak of gas release during unsteady-state devolatilizations of individual pellets. In this work, results were statistically analyzed by linear model regressions with the software R, assessing influences from: devolatilization temperature (700–900 °C), oxygen-carriers as bed-materials, biomass pretreatments (torrefaction, torrefaction-washing). For both integral-average and peak parameters, the temperature increase significantly augmented gas yield, carbon conversion and H_2/CO ratio. In comparison to previous deterministic studies of this group, the effects of oxygen-carriers and biomass pretreatments emerged more clearly. In addition, statistically-proved linear models were provided, for future simulations of devolatilizations of the investigated biomasses in chemical looping gasification from 700 °C to 900 °C.

1. Introduction

Statistical techniques of experimental design and data analyses proved to be useful in engineering, to discover new basic phenomena, develop new processes, improve existing products and processes (Montgomery and Runger, 2011). These techniques can lead to improved process yields, reduced process variability, closer conformance to nominal or target requirements, faster process design and development, decreased operating costs; in addition, the statistical approach allows the general control of variables and the screening of the most critical ones, ensuring the best process performance (Montgomery, 2017; Montgomery and Runger, 2011).

Chemical processes often involve complex nonlinear multivariate phenomena, with several factors significantly influencing the final outputs (Silva, 2018). Chemical engineering has successfully used, also at the industrial level, a wide set of statistical methodologies, ranging from descriptive approaches to complex optimization topics, always targeting safer, more repeatable, and profitable solutions (Montgomery, 2017).

As to diagnostic and control methods, data-driven fault detection has found applications in chemical processes (Luo et al., 2020; Nor et al., 2020), as well as principal component analysis (PCA) (Jollife and Cadima, 2016).

In the discipline of analysis, design and control of chemical processes, the design of experiments (DoE) represents a well-established method to systematically apply statistics to chemical experimentation and process development; it can be accompanied by statistical data treatments, often based on linear regressions (Tanco et al., 2009; Turcu et al., 2018).

That kind of applications was also used in the broad field of biomass gasification. (Lenis et al., 2013) used the analysis of variance (ANOVA) to study the effects of air flow, moisture, size and shape of biomass in a laboratory-scale gasifier. (Detchusananard et al., 2020) performed simulations by Aspen Plus of sorption-enhanced chemical looping gasification at process condition chosen by DoE, then applying response surface methodology (RSM) and ANOVA, and obtaining a multivariate linear regression model for optimization purposes. (Hanchate et al., 2021) adopted RSM to investigate the effect of superficial velocities on solid circulation rate in a dual fluidized bed gasifier, obtaining a

* Corresponding author.
E-mail address: katia.gallucci@univaq.it (K. Gallucci).

https://doi.org/10.1016/j.biteb.2021.100926
Received 13 December 2021; Received in revised form 15 December 2021; Accepted 15 December 2021
Available online 27 December 2021

regression model confirmed by ANOVA. (Hu et al., 2019) applied DoE to evaluate chemical looping gasification (CLG) performances of rice straw using a Fe-based oxygen carrier (OC), optimizing the production conditions by RSM to maximize H_2/CO ratio in the produced syngas.

This work applied a complete and balanced DoE to biomass devolatilizations in fluidized beds, performed as a preliminary propaedeutic study for their application in CLG based on the dual fluidized bed technology, in the framework of the Horizon 2020 project CLARA (chemical looping gasification for sustainable production of biofuels, G. A. 817841) (CLARA, 2021; The Concept: From Biomass to Biofuel – CLARA, 2021). Experimental results of that campaign have been published elsewhere (Di Giuliano et al., 2021a, 2021b; Lucantonio et al., 2021): overall, they concerned different devolatilization temperatures, types of wheat straw pellets (differently pretreated), types of fluidized bed materials (sand or three OCs). The influences from biomass pretreatments, nature of bed materials and process temperature on devolatilization performances were studied in those publications (Di Giuliano et al., 2021a, 2021b; Lucantonio et al., 2021), by a deterministic approach, which was not fully able to disclose and quantify those influences.

In this work, in order to perform a more systematic analysis of that devolatilization results and by virtue of the DoE based on an important amount of process variables, a statistical approach was used to get a deeper insight about experimental output, by means of a linear regression model. That approach ensured finding the statistically significant dependencies between considered input/output variables and provided a useful model for future scale-up studies of CLG based on pretreated wheat straw pellets. The developed algorithm integrates linear regression with homoskedasticity testing, data cleaning, and variable transformation, allowing a more standardized elaboration of experimental results.

2. Materials and methods

2.1. Experimental data

In previous publications (Di Giuliano et al., 2021a, 2021b; Lucantonio et al., 2021), devolatilizations of wheat straw pellets were performed in bubbling beds fluidized with N_2, as a preliminary and screening study for the application in CLG of differently pretreated biomasses and OCs. The gathering of data experimentally obtained in those publications (Di Giuliano et al., 2021a, 2021b; Lucantonio et al., 2021) constituted a complete and balanced DoE with three factors (type of "bed material", type of "biomass", devolatilization temperature T) at several levels (4, 7 and 3, respectively). Further specifications about those levels (i.e., pretreatments of wheat straw pellets, nature of bed materials, investigated values of T) and their nomenclature were detailed in Table 1, whereas details about the devolatilization test rig and related experimental procedures can be found elsewhere (Di Giuliano et al., 2021a; Lucantonio et al., 2021). Each experimental test under a set of operating conditions ("biomass/bed material/T") was carried out with 3 replications, totalizing 252 distinct tests.

Flow rate and composition of cooled and dried product gases were measured as functions of time for each devolatilized pellet. The resulting experimental outcomes (summarized in Table 1) were the integral-average values of gas yield (η^{av}), H_2/CO molar ratio in the outlet syngas (λ^{av}), biomass carbon conversion ($\chi_C{}^{av}$). In addition, the approach introduced by (Lucantonio et al., 2021) concerning "peak quantities" (study of maximum instantaneous flow rates of produced gases during each devolatilization, hereinafter denoted as "peak") was adopted to calculate peak molar fractions on a N_2-free basis, for H_2, CO, CO_2, CH_4 and other hydrocarbons cumulatively expressed as $C_3H_{8,eq}$ ($Y_{i,out}{}^{p}$ with i = H_2, CO, CO_2, CH_4 and $C_3H_{8,eq}$, Table 1). Further details about operation conditions and calculations of integral-average values and peak compositions can be found elsewhere (Di Giuliano et al., 2021a, 2021b; Lucantonio et al., 2021); all calculations are based on the principle of

Table 1
Experimental input and target/output/variables to develop the statistical linear regression model (OC = Oxygen Carrier, WSP = Wheat Straw Pellets).

Qualitative inputs	Name	Dummy value	Label Fig. 2	Description	Ref.
Bed material	Sand	/	1.0	Inert material	(Di Giuliano et al., 2021a)
	ILM	0 or 1	2.0	Ilmenite, mineral Fe—Ti oxide OC	(Condori et al., 2021a)
	SIB	0 or 1	4.0	"Sibelco" calcined, Mn—Fe based OC	(Di Giuliano et al., 2021a, 2020)
	LD	0 or 1	3.0	Slag from steelmaking Linz-Donawitz process, Fe-Mn-Ca based OC	(Hildor et al., 2020; Menad et al., 2014)
Biomass	WSP	/	1	Wheat Straw Pellet (i.e., pelletized wheat straw)	(Di Giuliano et al., 2021b, 2020)
	WSP-T1	0 or 1	2	WSP Torrefied at T1 = 250 °C	(Di Giuliano et al., 2020; Lucantonio et al., 2021)
	WSP-T1W	0 or 1	3	Washed WSP-T1	(Di Giuliano et al., 2020; Lucantonio et al., 2021)
	WSP-T2	0 or 1	4	WSP Torrefied at T2 = 260 °C	(Di Giuliano et al., 2020; Lucantonio et al., 2021)
	WSP-T2W	0 or 1	5	Washed WSP-T2	(Di Giuliano et al., 2020; Lucantonio et al., 2021)
	WSP-T3	0 or 1	6	WSP Torrefied at T3 = 270 °C	(Di Giuliano et al., 2020; Lucantonio et al., 2021)
	WSP-T3W	0 or 1	7	Washed WSP-T3	(Di Giuliano et al., 2020; Lucantonio et al., 2021)

Quantitative inputs	Symbol	Values	Description	Ref.
Devolatilization temperature (set-point)	T	700 °C 800 °C 900 °C	Set points temperature in devolatilization experiments	(Di Giuliano et al., 2021b; Lucantonio et al., 2021)
Effective temperature	T_{eff}	Directly measured values	Temperature at the quantitative maximum instantaneous peak of syngas release, traced by syngas flow rate as a function of time	
Integral-average parameters	η^{av}	Calculated experimental values	Integral-average gas yield ($mol_{gas}/g_{biomass}$)	(Di Giuliano et al., 2021b; Lucantonio et al., 2021)
	λ^{av}	Calculated experimental values	Integral-average H_2/CO molar ratio in the syngas (mol_{H2}/mol_{CO})	(Di Giuliano et al., 2021b; Lucantonio et al., 2021)
	$\chi_C{}^{av}$			(Di Giuliano et al.,

(continued on next page)

Table 1 (*continued*)

Quantitative inputs	Symbol	Values	Description	Ref.
		Calculated experimental values	Integral-average carbon conversion (%)	2021b; Lucantonio et al., 2021)
Peak compositions	$Y^{p}_{i,\ out}$	Calculated experimental values	Syngas composition on N_2-free basis expressed as molar fractions of *i-th* component, with $i = H_2$, CO, CO_2, CH_4 or hydrocarbons higher than CH_4 (cumulatively quantified as equivalent C_3H_8, "$C_3H_{8,eq}$"), determined at the maximum instantaneous peak of syngas release, traced by syngas flow rate as a function of time.	(Di Giuliano et al., 2021b; Lucantonio et al., 2021)

mass conservation and on the resulting molar balances (with N_2 as the internal standard in the gas phase). An additional experimental measurement was considered in the following statistical analysis, i.e., the effective bed temperature at the peak of syngas release (T_{eff}, Table 1).

2.2. Statistical analysis of experimental data

Integral-average values (η^{av}, λ^{av}, ${\chi_C}^{av}$) and peak molar fractions ($Y_{i,out}{}^{p}$ with $i = H_2$, CO, CO_2, CH_4 and $C_3H_{8,eq}$) have been discussed by following a deterministic approach in (Di Giuliano et al., 2021b) for the whole DoE: some correlations with the factors "biomass", "bed material", T were tricky to be deterministically identified, therefore a statistical linear regression model was applied here.

As for this model (Table 1): (i) the different types of "biomass" and "bed material" (qualitative variables), together with T and T_{eff} (quantitative variables), constituted the set of input variables; (ii) η^{av}, λ^{av}, ${\chi_C}^{av}$ and $Y_{i,out}{}^{p}$ (with $i = H_2$, CO, CO_2, CH_4 and $C_3H_{8,eq}$) were the target/output variables (all quantitative).

A first exploratory analysis of all available raw experimental data (see supplementary material) was performed by the "matrix of scatterplots". In each scatterplot, a couple of variables is displayed: scatterplots of the input variables vs. input variables (upper-left part of the matrix) give a visual representation of the experimental design; scatterplots combining input and target/output variables or couples of target/output variables provide a first idea on the nature of their relationships; finally, the presence of particularly anomalous values ("outliers") can be graphically identified.

To analyze the combined effect of input variables on the target/output variables (Table 1), a multiple-linear-regression-analysis approach was adopted, combining qualitative and quantitative input variables (also called regressors or explanatory variables). Linear regression analysis consists in finding the line which approximates the relationship between the considered variables and can be expressed, in formula, as (Mason et al., 2003; Meier and Zürich, 2013):

$$y_k = \beta_0 + \sum \beta_j X_{kj} + \varepsilon_k \tag{1}$$

where: y_k is the *k-th* out of m observations of a given target/output variable ($k = 1, \ldots, m$); y is the vector of the m observations; β_0 is the intercept term associated to the reference category; β_j is the coefficient associated to the *j-th* out of n explanatory variables ($j = 1, \ldots, n$); X is the matrix of regressors (one per column); and ε_k is the error term of y_k.

The interpretation of β_j changes according to the nature of the *j-th* regressor. If the column X_j corresponds to a quantitative input variable (e.g., T and T_{eff} in Table 1), then β_j represents the slope of the regressed line. If X_j corresponds to a qualitative input variable (e.g., "biomass" and "bed material" in Table 1) – declined as a series of categories (e.g. "SAND", "ILM", "SIB", "LD" for the input "bed material") – then X_j is expressed as set of dummy variables (i.e., a variable taking value 1 if the observation belongs to the category under consideration and 0 otherwise), and then β_j represents the shift in the intercept of the regressed line for the selected category, in comparison to the reference one (β_0). WSP (Table 1) in a bed made up of sand (Table 1) corresponds to β_0.

The error term ε_k expresses the non-deterministic nature of the model and incorporates residual/unexplained variability in y, including the effect of other unobservable factors. The assumptions for this non-deterministic approach are mainly composed of requirements about the distribution of ε_k (Eq. (2))

$$\varepsilon_k \overset{iid}{\sim} N\left(0; \sigma^2\right) \tag{2}$$

meaning that the errors must be independently and identically distributed (*iid*) with mean equal to 0 and constant variance σ^2 (the latter requirement referred to as "assumption of homoskedasticity"); the assumption of normal distribution (N) is not strictly necessary to compute the estimates of β_0 and β_j, but is required to perform inference on their significance. Moreover, the regressors must be exogenous, meaning that they should show no correlation with the error term.

Limits typically claimed about the linear regression models include: (i) their unsuitability to catch non-linear relationships; and (ii) their sensitivity to anomalous values (i.e., outliers). The former can be overcome with appropriate variable transformations (as attempted for $Y_{i,out}{}^{p}$ dependencies on T_{eff}). The latter was exploited to identify outliers, which – in the present case of study – resulted from either errors in data registration/transcription or occasionally uncontrolled experimental factors.

For each target/output variable (Table 1), the estimates of the related coefficients of the linear model were obtained by using ordinary least square (OLS) estimators, which are the solutions of the optimization problem in Eq. (3)

$$\begin{aligned} \widehat{\beta} &= \underset{\left(\widehat{\beta}_0, \widehat{\beta}_1, \ \ldots, \ \widehat{\beta}_j, \ldots, \ \widehat{\beta}_n\right)}{min} \sum \left(y_k - \widehat{\beta}_0 - \sum \widehat{\beta}_j X_{kj}\right)^2 \\ &= \underset{\left(\widehat{\beta}_0, \widehat{\beta}_1, \ \ldots, \ \widehat{\beta}_j, \ldots, \ \widehat{\beta}_n\right)}{min} \sum (d_k)^2 = \left(X_{ov}^T X_{ov}\right)^{-1} X_{ov}^T y \end{aligned} \tag{3}$$

where $\widehat{\beta}$ is the vector of the $n + 1$ estimates of coefficients of the model ($\widehat{\beta}_0$ and $\widehat{\beta}_j$ with $j = 1, \ldots, n$), X_{ov} is the overall matrix of the regressors (i.e., including X defined in Eq. (1) and a column of ones corresponding to the intercept). OLS estimates are those coefficient values that minimize the "residual sum of squares", where the residuals (d_k) represent the prediction errors of the model and are calculated as the difference between the actual/observed value (y_k) of the target/output variable and the one computed by the model ("fitted value" $\widehat{y}_k$) (Eq. (4)).

$$d_k = y_k - \widehat{y}_k = y_k - \left(\widehat{\beta}_0 + \sum \widehat{\beta}_j X_{kj}\right) \tag{4}$$

By virtue of the Gauss-Markov theorem, if the assumptions hold, OLS estimators have several appreciable properties, namely unbiasedness and minimum variance. To reduce the risk of violating crucial hypotheses, $\widehat{\beta}$ values for each target/output variable were obtained according to the flowchart detailed in Fig. 1:

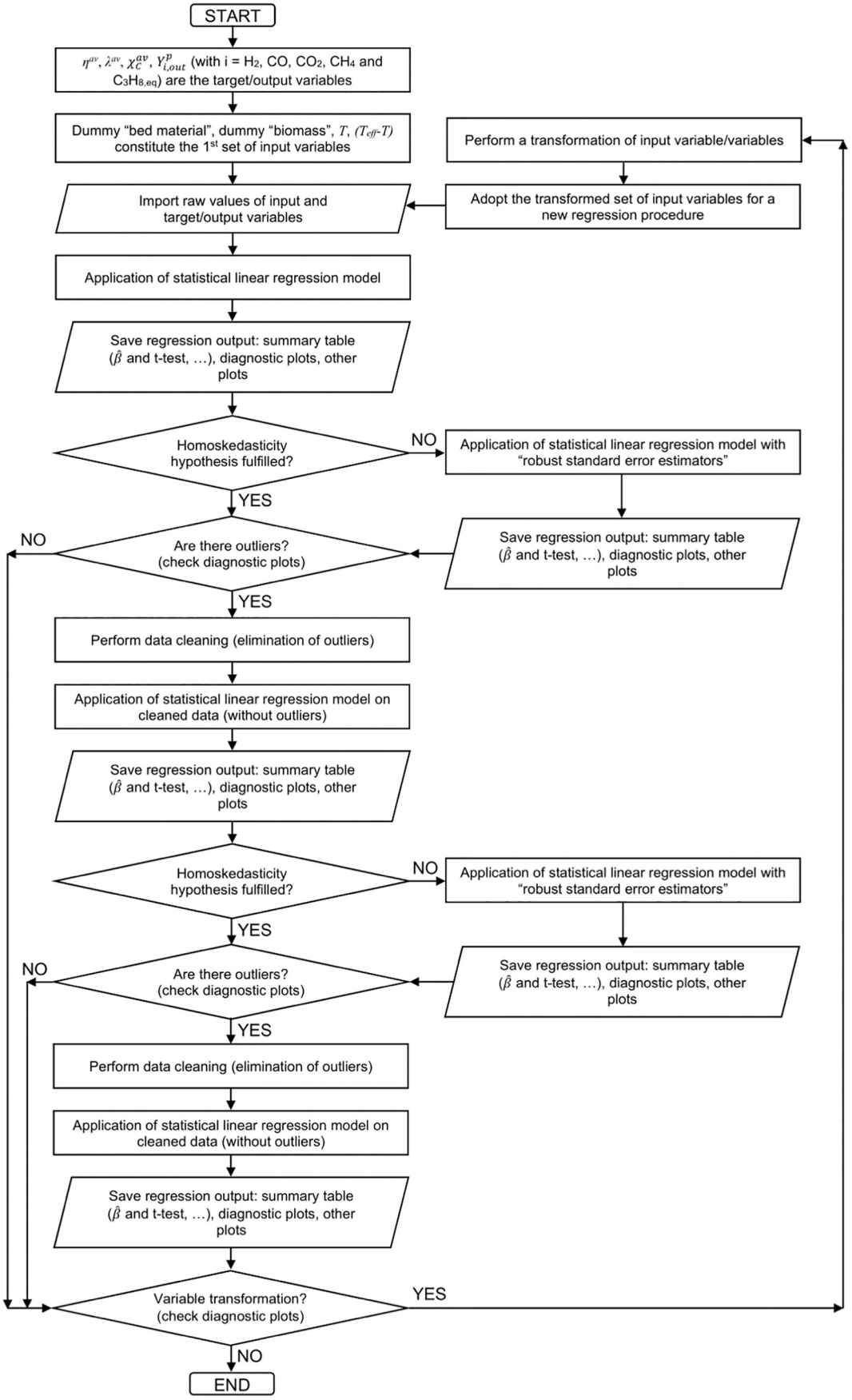

Fig. 1. Flowchart of regression operations.

- When homoskedasticity hypothesis resulted to be violated (by Breusch-Pagan test), "robust standard error estimators" were adopted to have solid significance evidence (White, 1980);
- To verify normality and independence assumptions (Eq. (2)), the outliers were identified by observing the "diagnostic plots" (Belsely et al., 1980) (see supplementary material) and the so-called "data cleaning" was carried out; "data cleaning" consisted of: (i) correcting errors in data registration/transcription; (ii) eliminating from the data set those observations for which no further correction was possible and with the Cook's distance greater than three times their average value (Identifying Outliers in Linear Regression — Cook's Distance [WWW Document], 2021);
- As a first attempt, for all assumed target/output variables, the following set of input variables were assumed (Table 1): (i) a dummy regressor for each level of the qualitative variable "bed material" other than the reference category "sand"; (ii) a dummy regressor for each level of the qualitative variable "biomass" other than the reference category WSP; (iii) the set-point devolatilization temperature T (700 °C, 800 °C, 900 °C); (iv) the deviation of effective temperature at the peak from the set-point, calculated as $(T_{eff} - T)$. When diagnostic plots suggested relationships with input variables other than first degree polynomial, a new set of input variables was tested (variable transformation).

The calculation of $\widehat{\beta}$ estimates by linear regressions was repeated

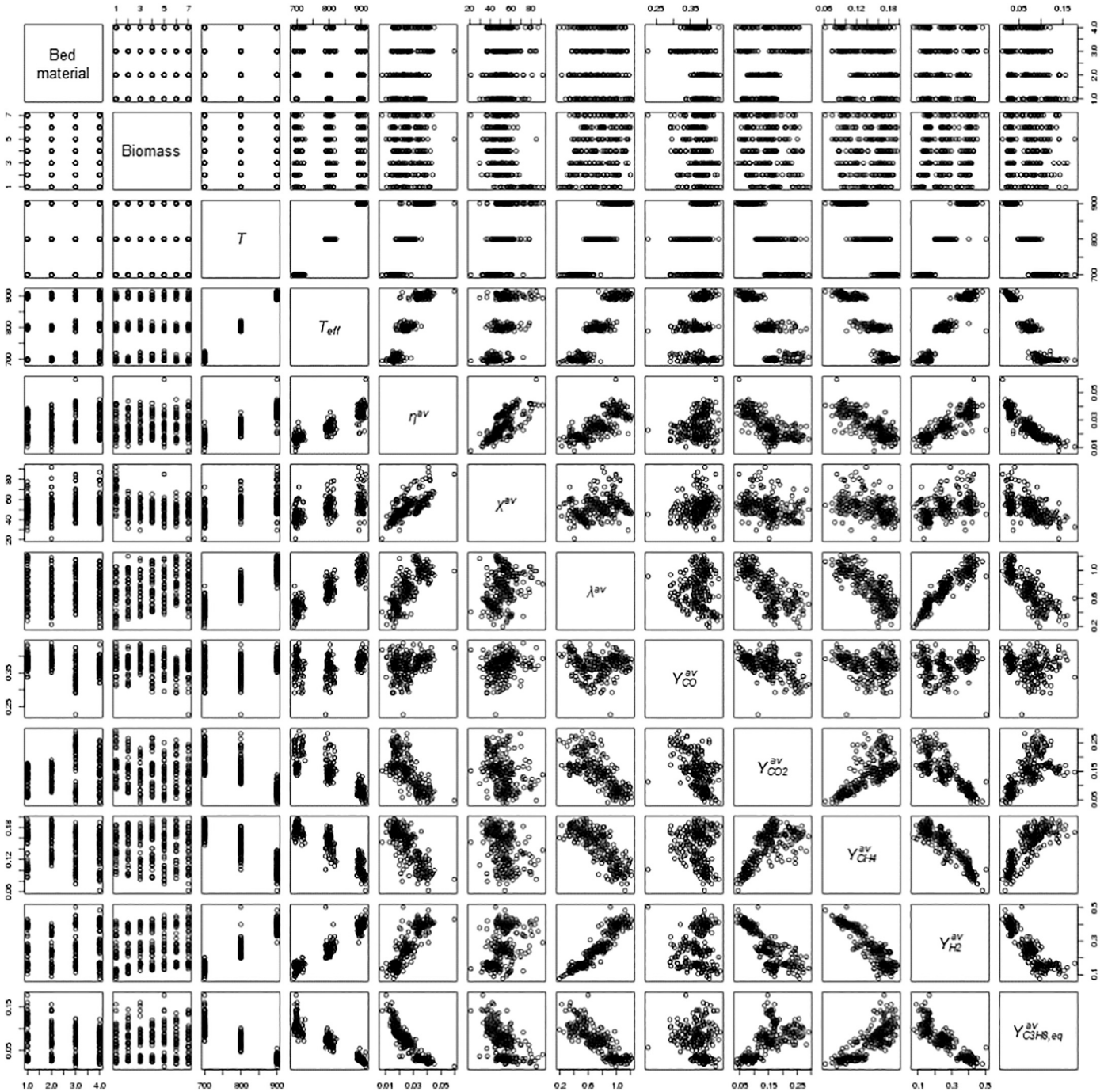

Fig. 2. Matrix of scatterplots of all the input and target/output variables. The meaning of numerical labels for "Bed" and "Biomass" factors is provided in Table 1.

whenever required by Fig. 1, for each target/output variable (Table 1). The statistical significance of $\widehat{\beta}$ estimates was evaluated by means of *t*-test statistic (see supplementary material).

The base version of the software R (R-Project, 2018) was always used, except for homoscedasticity testing and robust standard error estimators (by packages "lmtest" (Zeileis and Hothorn, 2002) and "sandwich" (Zeileis, 2004; Zeileis et al., 2020), respectively).

3. Results and discussion

3.1. Exploratory data analysis

Fig. 2 shows the matrix of scatterplots: it is a symmetric matrix in which the principal diagonal contains the names of all the variables included in the dataset (Table 1); each element above the principal diagonal shows the scatterplot of the variables identified by the corresponding column (x-axis) and row (y-axis) and the inverse graphs appear in the mirror element below the diagonal (row is the x-axis and column is the y-axis).

As mentioned in Section 2.2, the upper left part of the matrix in Fig. 2 displays correlations between couples of input variables (also listed Table 1). With regard to the three input variables which constituted the basis of the devolatilization DoE – "Bed material", "Biomass", and devolatilization temperature (*T*) – the related scatterplots confirmed that it was complete and balanced.

The visual analysis of T_{eff} as a function of *T* showed that deviations from the temperature set-point of experiments were limited, since no overlapping occurred between the three ranges of T_{eff} points (Fig. 2). This was also highlighted by descriptive analysis: the distribution of T_{eff} resulted to be centered on the corresponding *T* with a coefficient of variation of about 1% (ranging from 1.23% to 0.85% and decreasing for increasing values of *T*). In other words, the statistical analysis of the T_{eff} vs *T* scatterplot (Fig. 2) proved that the control of bed temperature during experimental tests was satisfying.

The scatterplots in the fourth column of Fig. 2, below T_{eff} (or their mirror images in the fourth row, on the right of T_{eff}) represented the influence of this input variable on all the target/output variables (Fig. 2): a clear increasing linear relationship appeared for gas yield (η^{av}), H_2 peak fraction ($Y_{H2,out}{}^{p}$) and outlet H_2/CO ratio (λ^{av}) as T_{eff} was increased, whereas a decreasing one was observed for $Y_{CH4,out}{}^{p}$, $Y_{CO2,out}{}^{p}$ and $Y_{C3H8eq,out}{}^{p}$; a less pronounced interdependence appeared between T_{eff} and carbon conversion ($\chi_C{}^{av}$); $Y_{CO,out}{}^{p}$ was apparently unaffected by the T_{eff}. Those behaviors of target/output variables vs T_{eff} are in quite good agreement with observations previously produced by the deterministic approach (Di Giuliano et al., 2021b) on raw experimental data (see supplementary material): H_2 appeared as a product of endothermic reactions which consume CH_4, CO_2 and other hydrocarbons ("$C_3H_{8,eq}$", see Table 1), such as dry and steam reforming, reverse water gas shift, reverse Boudouard, all thermodynamically favored as the process temperature is increased. On the other hand, the non-negligible presence of hydrocarbons suggested that devolatilized syngas was not at thermodynamic equilibrium, so it was sensible to assume that observed phenomena were regulated by a kinetic regime. As a matter of fact, the absence of a clear trend of $Y_{CO,out}{}^{p}$ along with T_{eff} did not find solid explanations by approaches based only on thermodynamic equilibria. On the other hand, it should also be considered that CO and CO_2 may be products of respectively uncomplete and complete combustions of carbonaceous compounds.

The remainder of the scatterplot matrix (Fig. 2) shows the relationships between target/output variables.

As to integral average parameters (Fig. 2), the gas yield (η^{av}) grew linearly along with carbon conversion ($\chi_C{}^{av}$) and outlet H_2/CO ratio (λ^{av}), with more dispersed data in the second case; data in the scatterplot between $\chi_C{}^{av}$ and λ^{av} did not follow recognizable functional paths, so evidencing no apparent mutual influences.

With regard to scatterplots coupling peak compositions ($Y_{i,out}{}^{p}$) in Fig. 2: a linearly decreasing relationship appeared between $Y_{H2,out}{}^{p}$ and $Y_{CH4,out}{}^{p}$, $Y_{CO2,out}{}^{p}$ and $Y_{C3H8eq,out}{}^{p}$, suggesting that the formerly proposed hypothesis about influences from dry reforming reactions or other decompositions of hydrocarbons may be consistent, and therefore that H_2 formation may be mainly ascribed to those conversions of hydrocarbons; $Y_{CO,out}{}^{p}$ appeared to decrease weakly as $Y_{CO2,out}{}^{p}$ increased (maybe an effect from water gas shift or oxidations promoted by OCs), whereas no correlations emerged with other syngas components.

When considering the crosslinking between integral-average parameters and peak compositions in Fig. 2, the overall absence of influences from the former on $Y_{CO,out}{}^{p}$ emerged, even with the H_2/CO ratio (λ^{av}); on the other hand, the growing $Y_{H2,out}{}^{p}$ seemed to linearly favor the increase of gas yield (η^{av}) and H_2/CO ratio (λ^{av}), which in turn may be ascribed to hydrocarbons decomposition and related CO_2 consumption in dry reforming. Weaker but similar relationships appeared for carbon conversion ($\chi_C{}^{av}$) and peak fractions of H_2, CH_4 and other hydrocarbons.

Influences between qualitative variables and target/outlet variables (listed in Table 1) are not fully inferable by scatterplots in Fig. 2, so the full statistical analysis by linear regression model was required.

As a last comment on Fig. 2, it is worth stressing how some outliers appeared; this fact did not affect the clear linearity of many relationships which supports the usage of a linear regression model, of which results are detailed in Section 3.2.

3.2. Results for the linear regression model

For each target/output variable (see Table 1), Table 2 summarizes the coefficient estimates of the statistical linear regression model (elements of vector $\widehat{\beta}$, Eq. (3)), after the data treatment described in Fig. 1. The most important feature of the statistical procedure described in Section 2.2, compared to the previous deterministic approach (Di Giuliano et al., 2021b) on raw experimental data (see supplementary material), is represented by data cleaning, which allowed the correction or elimination of any anomalous experimental point (outliers).

As a general consideration, the behavior of OCs may be affected by specific pre-activation procedures (e.g., activation with redox cycles or pre-oxidation of ilmenite (Abad et al., 2011), calcinations of LD-slags or ilmenite (Hildor et al., 2020)), as well as by process conditions (Tan et al., 2018) and CLG reactor configuration or scale (Condori et al., 2021a); as a consequence, trends commented in the following could be different from those found in the literature concerning CLG with OCs similar to those of this work (Condori et al., 2021b; Huijun et al., 2015; Moldenhauer et al., 2019; Wang et al., 2020).

3.2.1. Integral-average gas yield

The processing of gas yield (η^{av}) experimental results (see supplementary material) gave an example of the importance of data cleaning. The summary of the regression analysis for η^{av}, performed on raw experimental results (see supplementary material), suggested that the effects of both "bed material" and "biomass" variables were statistically indistinguishable from their reference categories (sand and WSP, respectively), with the sole exception of LD bed. However, related diagnostic plots Fig. 3(a)(b) indicated the presence of influent outliers. The correction/elimination of anomalous values allowed different significance evaluations: SIB emerged as significantly different from sand (*p*-value between 0.01 and 0.05, Table 2) on one side; on the other, WSP-T2W and WSP-T3 departed significantly from the reference WSP, while the acquired significance of WSP-T1 was more uncertain (p-value between 0.05 and 0.10, Table 2). The improvement due to data cleaning on η^{av} become also evident by a comparison of diagnostic plots (e.g., compare "Normal Q-Q" plots in Fig. 3(b) and (d).

As for regression outputs obtained with cleaned data of η^{av}: (i) the use of ILM was not statistically different from that of reference sand, while SIB and LD led to an increase of this target/output variable in

Table 2

Coefficients estimate of (elements of vector $\widehat{\beta}$, Eq. (3)) of the statistical linear regression model, for each target/output variable after the data treatment described in Fig. 1; subscript "0" means "reference state", i.e., WSP with sand; figures in parentheses under each reported coefficient estimate correspond to the p-value of the t-test, to be compared with the chosen significance level; as to coefficients with *p*-values >0.10 (10%) in the *t*-test, the related statistical correlation was assumed as surely "not significant" ("n.s.") and therefore related numerical values were not reported.

	η^{av}	$\chi_C{}^{av}$	λ^{av}	$Y_{CH4,out}{}^{p}$	$Y_{CO,out}{}^{p}$	$Y_{CO2,out}{}^{p}$	$Y_{H2,out}{}^{p}$	$Y_{C3H8eq,\ out}{}^{p}$
$\widehat{\beta}_0$	-5.227×10^{-2} ($< 2 \times 10^{-16}$)	$+1.068 \times 10^{1}$ (0.00463)	-1.560×10^{0} ($< 2 \times 10^{-16}$)	-4.660×10^{-1} (6.98×10^{-10})	$+3.540 \times 10^{-1}$ ($< 2 \times 10^{-16}$)	$+5.974 \times 10^{-1}$ ($< 2 \times 10^{-16}$)	$+3.042 \times 10^{-1}$ (0.03678)	$+3.7989 \times 10^{-1}$ ($< 2 \times 10^{-16}$)
$\widehat{\beta}_{ILM}$	n.s. (> 0.10)	n.s. (> 0.10)	-6.534×10^{-2} (8.51×10^{-7})	$+1.150 \times 10^{-2}$ (7.42×10^{-13})	n.s. (> 0.10)	$+1.489 \times 10^{-2}$ (2.877×10^{-6})	-2.010×10^{-2} (1.79×10^{-10})	-7.3131×10^{-3} (1.766×10^{-5})
$\widehat{\beta}_{SIB}$	$+1.105 \times 10^{-3}$ (0.03324)	n.s. (> 0.10)	-3.740×10^{-2} 0.00604 ()	-8.509×10^{-3} (6.41×10^{-8})	-1.357×10^{-2} ($< 2 \times 10^{-16}$)	$+2.583 \times 10^{-2}$ (5.252×10^{-16})	$+6.924 \times 10^{-3}$ (0.02612)	-1.1342×10^{-2} (1.210×10^{-9})
$\widehat{\beta}_{LD}$	$+1.529 \times 10^{-3}$ (0.00378)	n.s. (> 0.10)	n.s. (> 0.10)	-1.396×10^{-2} ($< 2 \times 10^{-16}$)	-4.981×10^{-2} (8.32×10^{-5})	$+5.925 \times 10^{-2}$ ($< 2 \times 10^{-16}$)	$+9.038 \times 10^{-3}$ (0.00391)	-8.0141×10^{-3} (5.384×10^{-6})
$\widehat{\beta}_{WSP-T1}$	-1.234×10^{-3} (0.06729)	-1.573×10^{1} ($< 2 \times 10^{-16}$)	$+9.081 \times 10^{-2}$ (3.57×10^{-7})	n.s. (> 0.10)	-1.030×10^{-2} (0.024636)	-2.922×10^{-2} (6.087×10^{-9})	$+1.952 \times 10^{-2}$ (2.13×10^{-6})	$+6.9985 \times 10^{-3}$ (0.0002828)
$\widehat{\beta}_{WSP-T2}$	n.s. (> 0.10)	-1.766×10^{1} ($< 2 \times 10^{-16}$)	$+1.287 \times 10^{-1}$ (2.14×10^{-12})	n.s. (> 0.10)	-1.518×10^{-2} (0.000827)	-2.634×10^{-2} (6.087×10^{-9})	$+3.238 \times 10^{-2}$ (5.08×10^{-14})	$+3.5128 \times 10^{-3}$ (0.0327435)
$\widehat{\beta}_{WSP-T3}$	-1.793×10^{-3} (0.00763)	-2.122×10^{1} ($< 2 \times 10^{-16}$)	$+1.951 \times 10^{-1}$ ($< 2 \times 10^{-16}$)	$+4.604 \times 10^{-3}$ (0.02055)	-2.533×10^{-2} (6.58×10^{-8})	-3.362×10^{-2} (3.427×10^{-11})	$+4.293 \times 10^{-2}$ ($< 2 \times 10^{-16}$)	$+5.6058 \times 10^{-3}$ (0.0014026)
$\widehat{\beta}_{WSP-T1W}$	n.s. (> 0.10)	-1.677×10^{1} ($< 2 \times 10^{-16}$)	$+4.704 \times 10^{-2}$ (0.00674)	-5.371×10^{-3} (0.00659)	$+1.454 \times 10^{-2}$ (0.001334)	-5.525×10^{-2} ($< 2 \times 10^{-16}$)	$+3.334 \times 10^{-2}$ (1.65×10^{-14})	$+7.0514 \times 10^{-3}$ (0.0004513)
$\widehat{\beta}_{WSP-T2W}$	-1.481×10^{-3} (0.03098)	-1.791×10^{1} ($< 2 \times 10^{-16}$)	$+1.120 \times 10^{-1}$ (3.43×10^{-10})	-5.359×10^{-3} (0.00864)	n.s. (> 0.10)	-4.972×10^{-2} ($< 2 \times 10^{-16}$)	$+4.381 \times 10^{-2}$ ($< 2 \times 10^{-16}$)	$+7.8123 \times 10^{-3}$ (6.492×10^{-5})
$\widehat{\beta}_{WSP-T3W}$	n.s. (> 0.10)	-1.779×10^{1} ($< 2 \times 10^{-16}$)	$+1.477 \times 10^{-1}$ (9.93×10^{-16})	-5.933×10^{-3} (0.00372)	n.s. (> 0.10)	-5.359×10^{-2} ($< 2 \times 10^{-16}$)	$+5.065 \times 10^{-2}$ ($< 2 \times 10^{-16}$)	$+3.6328 \times 10^{-3}$ (0.0960087)
$\widehat{\beta}_T$	$+9.839 \times 10^{-5}$ ($< 2 \times 10^{-16}$)	$+7.039 \times 10^{-2}$ ($< 2 \times 10^{-16}$)	$+2.775 \times 10^{-3}$ ($< 2 \times 10^{-16}$)	$+1.904 \times 10^{-3}$ ($< 2 \times 10^{-16}$)	$+4.530 \times 10^{-5}$ (0.003808)	-5.468×10^{-4} ($< 2 \times 10^{-16}$)	-1.446×10^{-3} (9.74×10^{-5})	-3.8503×10^{-4} ($< 2 \times 10^{-16}$)
$\widehat{\beta}_{(T_{eff}-T)}$	$+7.967 \times 10^{-5}$ (0.00110)	n.s. (> 0.10)	$+3.338 \times 10^{-3}$ (1.47×10^{-7})	$+1.743 \times 10^{-3}$ ($< 2 \times 10^{-16}$)	n.s. (> 0.10)	n.s. (> 0.10)	-1.566×10^{-3} (6.41×10^{-5})	-5.2210×10^{-4} (1.912×10^{-11})
$\widehat{\beta}_{(T_{eff})^2}$	/ /	/ /	/ /	-1.405×10^{-6} ($< 2 \times 10^{-16}$)	/ /	/ /	$+1.679 \times 10^{-6}$ (2.75×10^{-12})	/ /

Units of all $\widehat{\beta}$ values are those which make the statistical linear regression model consistent with the following units of input and target/output variables: °C for T, T_{eff}; $mol_{gas}/g_{biomass}$ for η^{av}; mol_{H2}/mol_{CO} for λ^{av}; % for $\chi_C{}^{av}$; $mol_i/mol_{N2\text{-}free}$ for $Y_{i,\ out}{}^{p}$ ($i = H_2$, CO, CO_2, CH_4 and $C_3H_{8,eq}$).

comparison to sand, more pronounced for LD ($\widehat{\beta}_{LD} = +1.529 \times 10^{-3}$ $mol_{gas}/g_{biomass} > \widehat{\beta}_{SIB} = +1.105 \times 10^{-3}$ $mol_{gas}/g_{biomass}$, Table 2); (ii) pretreatments on WSP, when statistically significant, caused a decrease of η^{av} (regressed coefficient estimates <0, the highest in absolute value obtained for WSP-T3, Table 2); (iii) the effect of devolatilization temperature, decomposed as that of T and the deviation $(T_{eff} - T)$, was always strongly significant, making η^{av} increase as the temperature was increased (Table 2). The negative effect of pretreatments on gas yield may be ascribed to torrefaction, which causes the preliminary separation of more labile volatiles.

In comparison to raw experimental data (see supplementary material), the cleaned linear regression allowed to get deeper insight concerning the effects of pretreatments on gas yield, also confirming intuitions about the more important influences due to the use of SIB or LD, and the overall effect of process temperature (Di Giuliano et al., 2021b).

3.2.2. Integral-average carbon conversion

With regard to carbon conversion ($\chi_C{}^{av}$), data cleaning (see supplementary material) did not affect the related main statistical outcomes; results from the linear regression model after data cleaning were summarized in Table 2.

None of the OCs was statistically different from sand, whereas all pretreatments strongly were (*p*-values of related coefficient estimates always $< 2 \times 10^{-16}$ in Table 2). All pretreatments determined a decrease of $\chi_C{}^{av}$ in comparison to the reference WSP, with related coefficient estimates (Table 2) in the range between - 15.73% ($\widehat{\beta}_{WSP-T1}$) and - 21.22% ($\widehat{\beta}_{WSP-T3}$). A deeper study of coefficient estimates related to "biomass" (Table 2) suggested that torrefaction of wheat straw pellets had the greatest impact on $\chi_C{}^{av}$, the higher the torrefaction temperature, the greater the reduction of $\chi_C{}^{av}$; conversely, the subsequent washing seemed to re-homogenize the behavior of pellets, whatever the torrefaction temperature was. As a matter of fact, the range mentioned just above was determined by WSP-T1 and WSP-T3, while coefficient estimates of torrefied-washed pellets (WSP-T1W, WSP-T2W, WSP-T3W) were closer to each other and not so far from the center of that range (Table 2).

Concerning temperature effects, noteworthy only T is strongly statistically significant ($\chi_C{}^{av}$ increased as T was increased, $\widehat{\beta}_T > 0$ in Table 2), whereas operational deviations due to the actual temperature control in the bed – i.e., $(T - T_{eff})$ – did not influenced the devolatilization outputs in terms of $\chi_C{}^{av}$.

As a consequence of these statistical observations, those inferences (Di Giuliano et al., 2021b) from raw experimental data (see supplementary material) which concerned the influences of OCs on $\chi_C{}^{av}$ should be handled carefully, whereas deterministic trends from raw experimental data (see supplementary material) which concerned biomass pretreatments and T well matched the statistical results of the cleaned linear regression for $\chi_C{}^{av}$.

3.2.3. Integral-average outlet H_2/CO molar ratio

In the case of outlet H_2/CO molar ratio (λ^{av}) too, the data cleaning did not heavily affect regression results (see supplementary material). Results of linear model regression for λ^{av} after data cleaning were summarized in Table 2.

As for the "bed material" input (Table 2), LD was not statistically significant, whereas the actions of SIB and ILM determined a decrease of λ^{av} in comparison to reference sand; the most significant and quantitatively important "bed material" effect was due to ILM ($\widehat{\beta}_{ILM} = -6.534 \times 10^{-2}$ mol_{H2}/mol_{CO}, Table 2).

All biomass pretreatments determined a statistically significant increase of λ^{av} in comparison to raw WSP (coefficient estimates >0 and *p*-values always <0.01, Table 2). A correlation emerged between torrefaction temperature and estimated coefficients, for both torrefied and torrefied-washed pellets (Table 2): the higher that temperature, the higher the increase of λ^{av} in comparison to WSP; this evidence is in good agreement with the analysis of peak ratios $Y_{H2,out}{}^{p}/Y_{CO,out}{}^{p}$ performed by

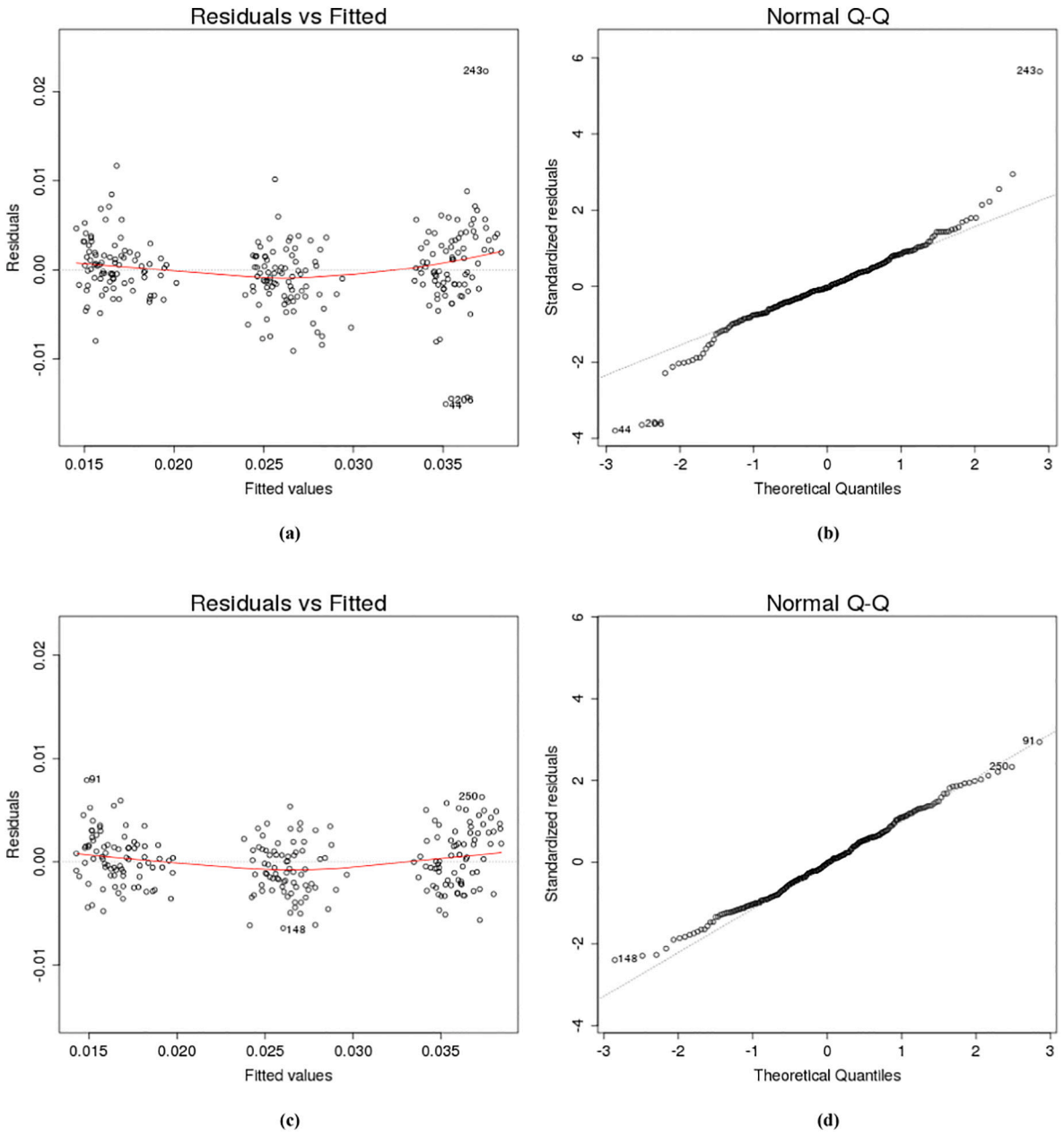

Fig. 3. Diagnostic plots of the regression analysis for gas yield (η^{av}): Residual vs. fitted plot before data cleaning (a); Normal Q-Q plot before data cleaning before data cleaning (b) Residual vs. fitted plot data after data cleaning (c); Normal Q-Q plot after data cleaning after data cleaning (d); for further details (see supplementary material).

(Di Giuliano et al., 2021b; Lucantonio et al., 2021) based on raw experimental data (see supplementary material). In addition, being the torrefaction temperature equal, torrefied pellets always had a regressed coefficient estimate higher than that of homologous torrefied-washed version (Table 2). As a consequence, the most important increase of λ^{av} was ascribed to WSP-T3 ($\widehat{\beta}_{WSP-T3} = +1.951 \times 10^{-1}$ mol_{H2}/mol_{CO}, Table 2).

The effects of both T and $(T - T_{eff})$ resulted as statistically significant (see related p-values in Table 2), both with positive coefficient estimates; in other words, the increase of process temperature favored the increase of λ^{av}. This evidence well matches the hypotheses about the promotion of H_2 production due to endothermic reactions, discussed in Section 3.1 on the basis of scatterplots (Fig. 2), as well as the deterministic observations of raw experimental data (see supplementary material) obtained by (Di Giuliano et al., 2021b).

3.2.4. Peak compositions

After the regression with all input variables as first-degree polynomial (Fig. 1), a variable transformation attempt was performed for all $Y_{i,out}^{p}$ (with $i = H_2$, CO, CO_2, CH_4 and $C_3H_{8,eq}$), by adding a dependence on the quadratic term T_{eff}^{2} in the regression linear model. This decision descended from the clear non-linear pattern obtained in the "Residual vs Fitted" plots for $Y_{H2,out}^{p}$ (Fig. 4(a)) and $Y_{CH4,out}^{p}$ (Fig. 5(a)) by the first regression with all input variables as first-degree polynomial, even after data cleaning. The introduction of T_{eff}^{2} in the regression caused a net improvement in the distribution of "Residual vs Fitted" plots for $Y_{H2,out}^{p}$ (Fig. 4(c)) and $Y_{CH4,out}^{p}$ (Fig. 5(c)), leading to choose the model with T_{eff}^{2} for H_2 and CH_4. In the cases of CO, CO_2 and C_3H_{8eq}, the need of that variable transformation was not equally evident (see supplementary material), but was performed as a countercheck: a comparison of "Residual vs Fitted" plots with and without the T_{eff}^{2} dependency did not highlight significant improvements (see supplementary material), so the

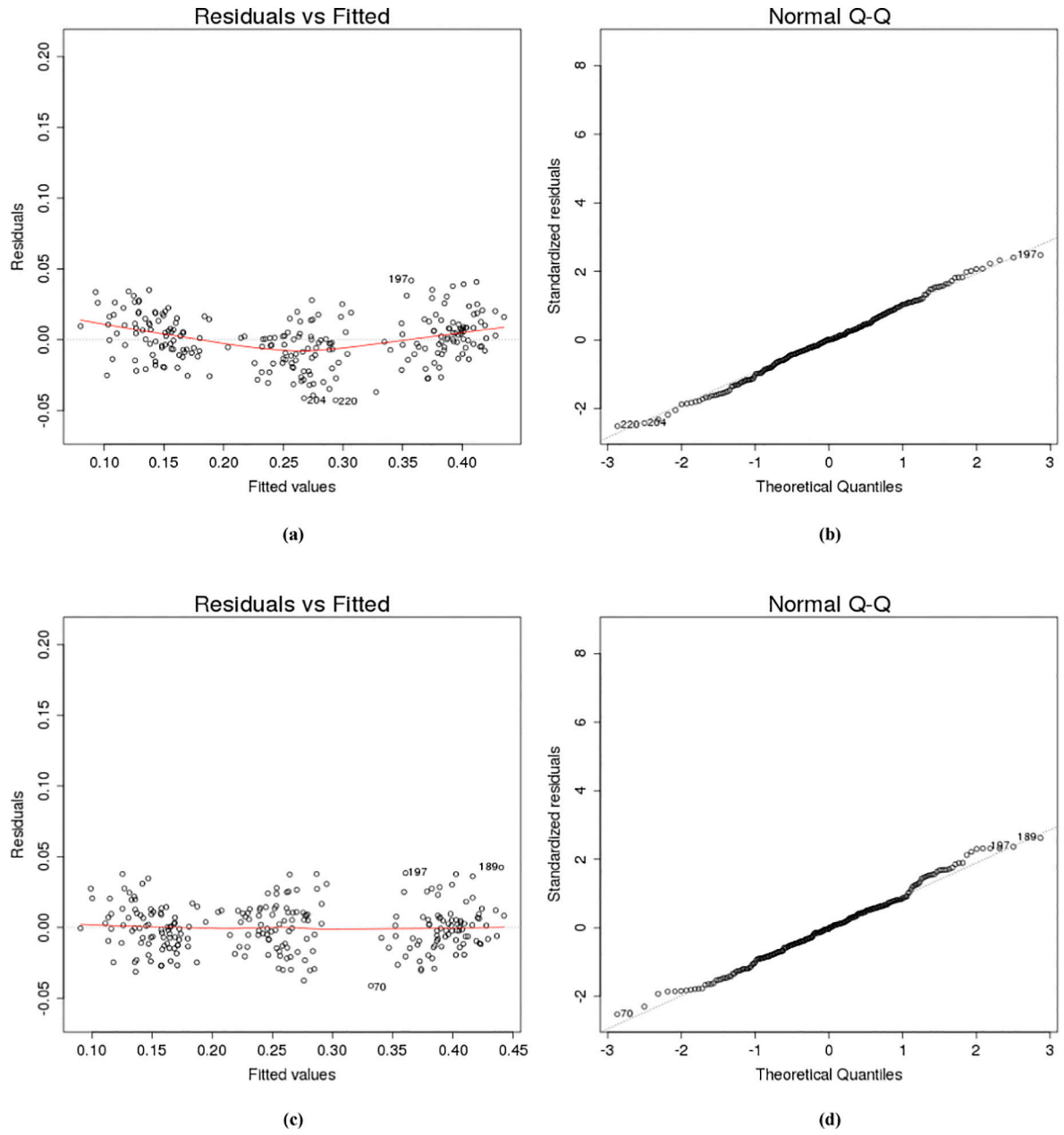

Fig. 4. Diagnostic plots of the regression analysis for peak H_2 molar fraction on N_2-free basis ($Y_{H2,out}{}^{p}$): Residual vs. fitted plot after the first data cleaning (a); Normal Q-Q plot after the first data cleaning (b); Residual vs. fitted plot after adding linear dependence on $T_{eff}{}^{2}$ and the following data cleaning (c); Normal Q-Q plot after adding linear dependence on $T_{eff}{}^{2}$ and the following data cleaning (d); for further details (see supplementary material).

simpler model was kept for $Y_{CO,out}{}^{p}$, $Y_{CO2,out}{}^{p}$ and $Y_{C3H8eq,out}{}^{p}$.

As to $Y_{H2,out}{}^{p}$, the regressed coefficient estimates (Table 2) were statistically significant for all considered qualitative and quantitative variables. ILM determined the decrease of $Y_{H2,out}{}^{p}$ in comparison to sand ($\widehat{\beta}_{ILM} = -2.010 \times 10^{-2}$ $mol_{H2}/mol_{N2\text{-}free}$), higher in absolute value than the increase obtained by SIB ($\widehat{\beta}_{SIB} = +6.924 \times 10^{-3}$ $mol_{H2}/mol_{N2\text{-}free}$) or LD ($\widehat{\beta}_{LD} = +9.038 \times 10^{-3}$ $mol_{H2}/mol_{N2\text{-}free}$). All pretreatments on WSP allowed increasing $Y_{H2,out}{}^{p}$ (coefficient estimates >0, Table 2), with strong statistical significance (*p*-values of *t*-test in the range 0–0.001, Table 2): for both torrefied and torrefied-washed biomasses, the higher the torrefaction temperature the more conspicuous the increase of $Y_{H2,out}{}^{p}$ (see related $\widehat{\beta}$ estimates in Table 2); being the torrefaction temperature equal, the torrefied-washed biomasses always had a higher $\widehat{\beta}$ estimate than those of only torrefied biomasses (Table 2). As to torrefaction temperature, (Zhang et al., 2021) performed pyrolysis tests with thermogravimetric-analysis (TGA) on Fe_2O_3 mixed with spruce-pine-fir, torrefied at different temperatures in the range 240–330 °C: they found a maximum of H_2 content in released syngas with their residual biomass torrefied at 270 °C (equal to "T3" of this work, Table 1), corresponding to a minimum activation energy of H_2 release in their kinetic analysis. With regard to torrefaction and torrefaction-washing, (Zhang et al., 2015) applied these pretreatments to rice husk, pyrolyzed by a microwave assisted process at 550 °C: they found a substantial increase of H_2 fraction in the devolatilized syngas for both their torrefied and torrefied-washed samples, when compared to rice husk in raw state or only washed with water; conversely to wheat straw tested here, (Zhang et al., 2015) found slightly higher H_2 fractions for only-torrefied samples. Other studies about washing (Carrillo et al., 2014) determined that this pretreatment increases the biomass quality and its volatiles matter. The different behavior of ILM in comparison to SIB and LD qualitatively emerged also by the previous (Di Giuliano et al., 2021b)

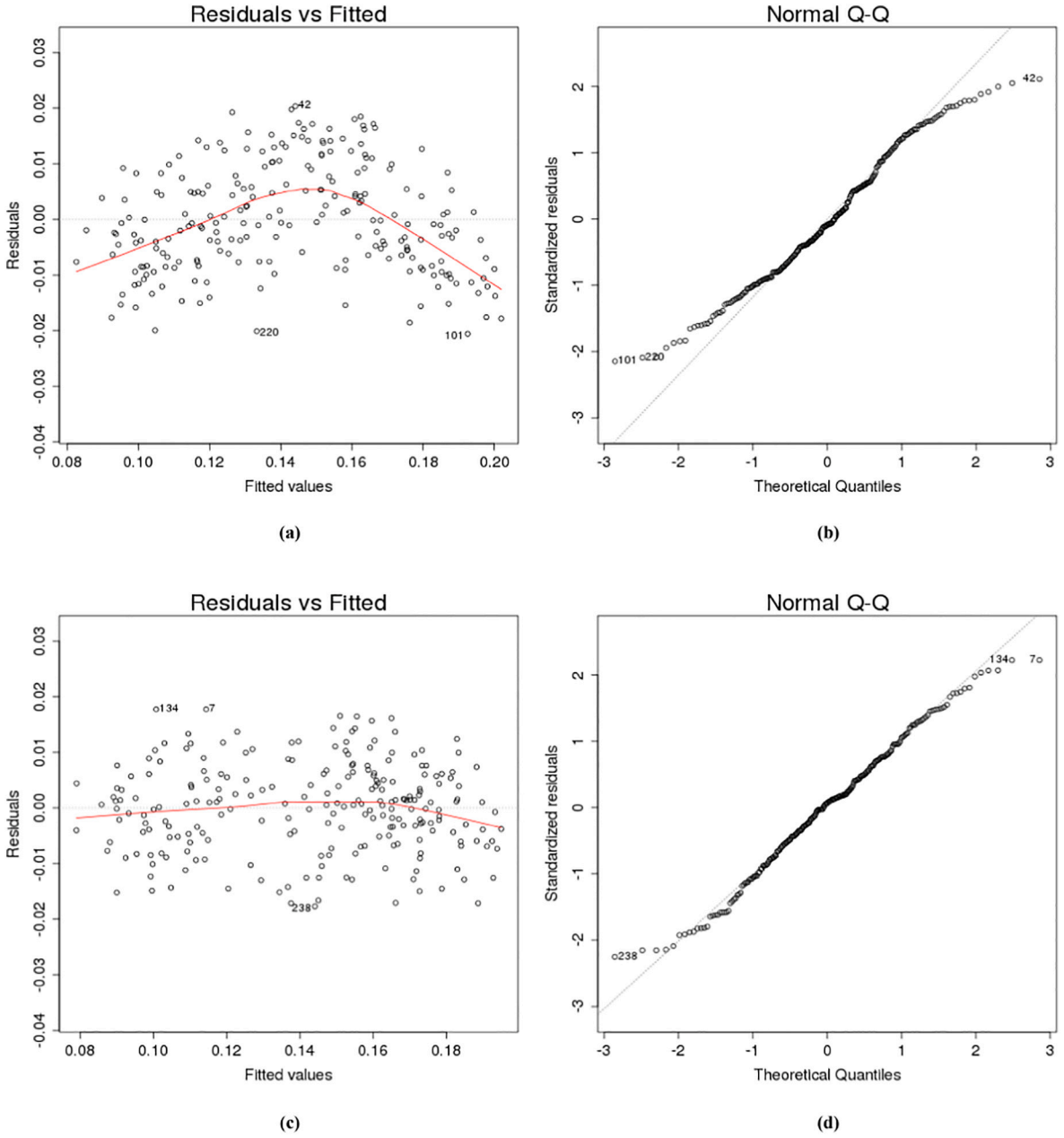

Fig. 5. Diagnostic plots of the regression analysis for peak CH_4 molar fraction on N_2-free basis ($Y_{CH4,out}{}^{p}$): Residual vs. fitted plot after the first data cleaning (a); Normal Q-Q plot after the first data cleaning (b); Residual vs. fitted plot after adding linear dependence on $T_{eff}{}^{2}$ and the following data cleaning (c); Normal Q-Q plot after adding linear dependence on $T_{eff}{}^{2}$ and the following data cleaning (d); for further details (see supplementary material).

deterministic analyses of raw experimental data (see supplementary material), as well as the improvements in H_2 development due to pretreatments. As to process temperature, all the three terms *T*, $(T_{eff} - T)$ and $T_{eff}{}^{2}$ were significant, with *p*-values always lower than 0.0001 (Table 2).

With regard to $Y_{CH4,out}{}^{p}$, in the linear model with dependence on $T_{eff}{}^{2}$ (Table 2), all OCs resulted as statistically different from sand, whereas only some pretreatments determined significant differences from reference WSP. $\widehat{\beta}$ values of "bed material" categories had opposite signs in comparison to those obtained for $Y_{H2,out}{}^{p}$(Table 2), in agreement with the hypothesis about H_2 production correlated to the conversion of CH_4. Effects of torrefaction-washing in comparison to WSP usage may be sensibly evaluated as significant, thanks to their p-values (always <0.01, Table 2); related coefficient estimates were always negative (Table 2), indicating a lower fraction of CH_4 developed in comparison to WSP. Depending on the significance level chosen, WSP-T3 may become significant too, while torrefaction at T1 and T2 are definitively not statistically different in comparison to WSP, as for CH_4 fraction (Table 2). Those effects from "biomass" and "bed material" categories were not inferable by the deterministic analysis of raw experimental data (see supplementary material) done by (Di Giuliano et al., 2021b). As to process temperature, all the three terms *T*, $(T_{eff} - T)$ and $T_{eff}{}^{2}$ were very significant, with p-values always practically null (Table 2).

Concerning $Y_{CO,out}{}^{p}$, regression results assessed the already observed (Fig. 2) weaker influence from process temperature; as a matter of fact and contrary to H_2, CH_4 and C_3H_{8eq}, the deviations $(T_{eff} - T)$ were not statistically significant for CO peak fraction (Table 2). The substitution of sand with OCs produced appreciable changes only with SIB and LD, in both cases with the decrease of $Y_{CO,out}{}^{p}$, more important for LD ($\widehat{\beta}_{LD} = -4.981 \times 10^{-2}$ $mol_{CO}/mol_{N2\text{-}free}$). This last evidence matched well the

hypothesis of promotion of water gas shift reaction due to carbonation of CaO in LD at the lowest tested temperature, proposed by (Di Giuliano et al., 2021b). Torrefaction determined the decrease of $Y_{CO,out}^{p}$ in comparison to syngas from WSP devolatilization, the higher the torrefaction temperature the more important that decrease (Table 2), as also occurred for devolatilization of other torrefied residual biomasses (Zhang et al., 2021, 2015). Among torrefied-washed biomasses, only WSP-T1W was statistically different from WSP, as far as peak CO fraction is concerned (Table 2).

As for $Y_{CO2,out}^{p}$, the significance of coefficient estimates related to temperature effects was analogous to that already commented for CO (Table 2); $\widehat{\beta}_T$ for $Y_{CO2,out}^{p}$ was negative, relevantly with opposite sign in comparison to the homologous coefficient of $Y_{CO,out}^{p}$ (Table 2). This fact may be ascribed to exothermic reactions involving CO and CO_2 (water gas shift, Boudouard equilibrium, combustion in presence of OCs). The use of all three OCs determined the statistically significant increase of CO_2 fraction, in comparison to reference tests with sand, with the most influent effect due to LD ($\widehat{\beta}_{LD} = +\ 5.925 \times 10^{-2}$ $mol_{CO2}/mol_{N2\text{-}free}$ Table 2). The pretreatments were all significant and always involved lower $Y_{CO2,out}^{p}$ in comparison to WSP, in good agreement with deterministic observations on raw experimental data (see supplementary material) (Di Giuliano et al., 2021b) and with microwave assisted pyrolysis on torrefied and torrefied-washed residual biomass from (Zhang et al., 2015).

As for $Y_{C3H8eq,out}^{p}$, the use of OCs in the place of sand was always statistically significant, involving a reduction of the fractions of hydrocarbons other than CH_4, a fact ascribable to the expected oxidizing action of these materials; SIB was the most influent OC ($\widehat{\beta}_{SIB} = -\ 1.1342 \times 10^{-2}$ $mol_{C3H8eq}/mol_{N2\text{-}free}$, Table 2). All pretreatments determined an increase of hydrocarbons cumulated as C_3H_{8eq}, in comparison to the reference case of WSP (Table 2); the torrefaction and torrefaction-washing pretreatments may have left in biomass pellets those carbonaceous compounds which were slightly more recalcitrant to thermochemical conversions. (Zhang et al., 2016) verified this for a different residual biomass, by TGA experiments: water-washing increased the initial decomposition temperature (T_i) and the temperature of maximum loss rate (T_{max}) of rice husk; the addition of torrefaction to water-washing furtherly increased T_i (the higher the torrefaction temperature, the higher T_i); in other words, the thermal stability of samples tested in TGA has been enhanced by both water-washing and torrefaction. In previous deterministic analyses (Di Giuliano et al., 2021b) of raw devolatilization data (see supplementary material), the effects from OCs on hydrocarbons were slightly evident only at 700 °C and those from biomasses were not clear. $Y_{C3H8eq,out}^{p}$ appreciably depended on both T and $(T_{eff} - T)$, decreasing as the process temperature was increased.

4. Conclusions

A linear regression model for devolatilization gaseous products – expressing dependencies on process temperature, bed and biomass natures – was obtained from experimental data. Statistically, the higher the process temperature (700–900 °C) the higher the gas yield, the carbon conversion, the outlet H_2/CO ratio and H_2 fraction, and the lower the fractions of CO_2, CH_4, other hydrocarbons. Compared to sand, oxygen carriers were not always statistically different, but their oxidizing action was statistically sensible. Torrefaction and torrefaction-washing involved statistically significant decreases of gas yields and carbon conversions; the highest torrefaction temperature (270 °C) involved the highest increase of H_2/CO ratios and H_2 fractions.

Funding

This research was funded by the Horizon 2020 Framework program of the European Union, CLARA project, G.A. 817841.

CRediT authorship contribution statement

Andrea Di Giuliano: Conceptualization, Methodology, Validation, Formal analysis, Investigation, Data curation, Writing – original draft, Writing – review & editing, Visualization, Supervision. **Marta Gallucci:** Conceptualization, Methodology, Software, Validation, Formal analysis, Investigation, Data curation, Writing – original draft, Writing – review & editing, Visualization, Supervision. **Barbara Malsegna:** Investigation, Data curation, Writing – original draft, Writing – review & editing. **Stefania Lucantonio:** Investigation, Data curation, Writing – original draft, Writing – review & editing. **Katia Gallucci:** Conceptualization, Methodology, Validation, Formal analysis, Investigation, Resources, Data curation, Writing – original draft, Writing – review & editing, Supervision, Project administration, Funding acquisition.

Declaration of competing interest

The authors declare that they have no known competing financial interests or personal relationships that could have appeared to influence the work reported in this paper. Marta Gallucci declares that the present work was carried out on a personal basis and does not involve the responsibility of her institution “Agenzia delle Entrate".

Acknowledgements

The provision of biomass pellets by National Renewable Energy Centre of Spain (CENER) and of oxygen carriers by Chalmers University of Technology (Göteborg, Sweden) is acknowledged, both CLARA partners.

Appendix A. Supplementary data

Supplementary data to this article can be found online at https://doi.org/10.1016/j.biteb.2021.100926.

References

Abad, A., Adánez, J., Cuadrat, A., García-Labiano, F., Gayán, P., de Diego, L.F., 2011. Kinetics of redox reactions of ilmenite for chemical-looping combustion. Chem. Eng. Sci. 66, 689–702. https://doi.org/10.1016/J.CES.2010.11.010.

Belsely, D.A., Kuh, E., Welsh, E.R., 1980. Regression Diagnostics: Identifying Influential Data and Sources of Collinearity. New York. https://doi.org/10.1002/0471725153.

Carrillo, M.A., Staggenborg, S.A., Pineda, J.A., 2014. Washing sorghum biomass with water to improve its quality for combustion. Fuel 116, 427–431. https://doi.org/10.1016/J.FUEL.2013.08.028.

CLARA, 2021. Chemical looping gasification for sustainable production of biofuels [WWW Document]. https://clara-h2020.eu/ (accessed 9.3.21).

Condori, O., García-Labiano, F., de Diego, L.F., Izquierdo, M.T., Abad, A., Adánez, J., 2021a. Biomass chemical looping gasification for syngas production using ilmenite as oxygen carrier in a 1.5 kWth unit. Chem. Eng. J. 405 https://doi.org/10.1016/j.cej.2020.126679.

Condori, O., García-Labiano, F., de Diego, L.F., Izquierdo, M.T., Abad, A., Adánez, J., 2021b. Biomass chemical looping gasification for syngas production using LD Slag as oxygen carrier in a 1.5 kWth unit. Fuel Process. Technol. 222, 106963 https://doi.org/10.1016/J.FUPROC.2021.106963.

Detchusananard, T., Im-orb, K., Maréchal, F., Arpornwichanop, A., 2020. Analysis of the sorption-enhanced chemical looping biomass gasification process: performance assessment and optimization through design of experiment approach. Energy 207, 1–11. https://doi.org/10.1016/j.energy.2020.118190.

Di Giuliano, A., Funcia, I., Pérez-Vega, R., Gil, J., Gallucci, K., 2020. Novel application of pretreatment and diagnostic method using dynamic pressure fluctuations to resolve and detect issues related to biogenic residue ash in chemical looping gasification. Processes 8. https://doi.org/10.3390/PR8091137.

Di Giuliano, A., Lucantonio, S., Gallucci, K., 2021a. Devolatilization of residual biomasses for chemical looping gasification in fluidized beds made up of oxygen-carriers. Energies 14, 311. https://doi.org/10.3390/en14020311.

Di Giuliano, A., Lucantonio, S., Malsegna, B., Gallucci, K., 2022. Pretreated residual biomasses in fluidized beds for chemical looping Gasification: experimental devolatilizations and characterization of ashes behavior. Bioresour. Technol. 345, 126514 https://doi.org/10.1016/j.biortech.2021.126514.

Hanchate, N., Malhotra, R., Mathpati, C.S., 2021. Design of experiments and analysis of dual fluidized bed gasifier for syngas production: cold flow studies. Int. J. Hydrog. Energy 46, 4776–4787. https://doi.org/10.1016/J.IJHYDENE.2020.02.114.

Hildor, F., Leion, H., Linderholm, C.J., Mattisson, T., 2020. Steel converter slag as an oxygen carrier for chemical-looping gasification. Fuel Process. Technol. 210, 106576 https://doi.org/10.1016/j.fuproc.2020.106576.

Hu, J., Li, C., Lee, D.J., Guo, Q., Zhao, S., Zhang, Q., Li, D., 2019. Syngas production from biomass using Fe-based oxygen carrier: optimization. Bioresour. Technol. 280, 183–187. https://doi.org/10.1016/J.BIORTECH.2019.02.012.

Huijun, G., Laihong, S., Fei, F., Shouxi, J., 2015. Experiments on biomass gasification using chemical looping with nickel-based oxygen carrier in a 25 kWth reactor. Appl. Therm. Eng. 85, 52–60. https://doi.org/10.1016/J.APPLTHERMALENG.2015.03.082.

Identifying Outliers in Linear Regression — Cook's Distance [WWW Document]. https://towardsdatascience.com/identifying-outliers-in-linear-regression-cooks-distance-9e212e9136a, 2021 (accessed 10.19.21).

Jollife, I.T., Cadima, J., 2016. Principal component analysis: a review and recent developments. Philos. Trans. R. Soc. A Math. Phys. Eng. Sci. 374 https://doi.org/10.1098/rsta.2015.0202.

Lenis, Y.A., Agudelo, A.F., Pérez, J.F., 2013. Analysis of statistical repeatability of a fixed bed downdraft biomass gasification facility. Appl. Therm. Eng. 51, 1006–1016. https://doi.org/10.1016/j.applthermaleng.2012.09.046.

Lucantonio, S., Di Giuliano, A., Gallucci, K., 2021. Influences of the pretreatments of residual biomass on gasification processes: experimental devolatilizations study in a fluidized bed. Appl. Sci. 11, 5722. https://doi.org/10.3390/app11125722.

Luo, L., Wang, J., Tong, C., Zhu, J., 2020. Multivariate fault detection and diagnosis based on variable grouping. Ind. Eng. Chem. Res. https://doi.org/10.1021/acs.iecr.0c00192.

Mason, R.L., Gunst, R.F., Hess, J.L., 2003. Statistical Design and Analysis of experiments: With applications to Engineering and Science, 2nd ed. John Wiley & sons, Hoboken, New Jersey.

Meier, L., Zürich, E., 2013. Statistical and Numerical Methods for Chemical Engineers part on Statistics.

Menad, N., Kanari, N., Save, M., 2014. Recovery of high grade iron compounds from LD slag by enhanced magnetic separation techniques. Int. J. Miner. Process. 126, 1–9. https://doi.org/10.1016/j.minpro.2013.11.001.

Moldenhauer, P., Linderholm, C., Rydén, M., Lyngfelt, A., 2019. Avoiding CO2 capture effort and cost for negative CO2 emissions using industrial waste in chemical-looping combustion/gasification of biomass. Mitig. Adapt. Strateg. Glob. Chang. 251 (25), 1–24. https://doi.org/10.1007/S11027-019-9843-2.

Montgomery, D.C., 2017. Design and Analysis of experiments, 9th ed. John Wiley & sons.

Montgomery, D.C., Runger, G.C., 2011. Applied Statistics and Probability.

Nor, N.M., Hassan, C.R.C., Hussain, M.A., 2020. A review of data-driven fault detection and diagnosis methods: applications in chemical process systems. Rev. Chem. Eng. 36, 513–553. https://doi.org/10.1515/REVCE-2017-0069.

R-Project, 2018. The R Project for Statistical Computing.

Silva, V., 2018. Statistical Approaches with Emphasis on Design of Experiments Applied to Chemical Processes. https://doi.org/10.5772/65616.

Tan, Y., Sun, Z., Cabello, A., Lu, D.Y., Hughes, R.W., 2018. Effects of H2S on the reactivity of ilmenite ore as chemical looping combustion oxygen carrier with methane as fuel. Energy Fuel 33, 585–594. https://doi.org/10.1021/ACS.ENERGYFUELS.8B03012.

Tanco, M., Viles, E., Ilzarbe, L., Alvarez, M.J., 2009. Implementation of design of experiments projects in industry. Appl. Stoch. Model. Bus. Ind. 25, 478–505. https://doi.org/10.1002/asmb.779.

The Concept: From Biomass to Biofuel – CLARA [WWW Document]. https://clara-h2020.eu/the-concept/, 2021 (accessed 8.1.21).

Turcu, A.M., Ghica, V.G., Veglio, F., Buzatu, M., Petrescu, M.I., Iacob, G., Bîrloagă, I., 2018. Catalytic paste solubilization researches regarding the cobalt recovery from used li-ion batteries - Anova application. UPB SciBull. Ser. B Chem. Mater. Sci. 80, 183–194.

Wang, S., Song, T., Yin, S., Hartge, E.U., Dymala, T., Shen, L., Heinrich, S., Werther, J., 2020. Syngas, tar and char behavior in chemical looping gasification of sawdust pellet in fluidized bed. Fuel 270, 117464. https://doi.org/10.1016/J.FUEL.2020.117464.

White, H., 1980. A heteroskedasticity-consistent covariance matrix estimator and a direct test for heteroskedasticity. Econometrica 48, 817. https://doi.org/10.2307/1912934.

Zeileis, A., 2004. Econometric computing with HC and HAC covariance matrix estimators. J. Stat. Softw. 11, 1–17. https://doi.org/10.1002/wics.10.

Zeileis, A., Hothorn, T., 2002. Diagnostic checking in regression relationships. R News 2, 7–10.

Zeileis, A., Köll, S., Graham, N., 2020. Various versatile variances: an object-oriented implementation of clustered covariances in r. J. Stat. Softw. 95, 1–36. https://doi.org/10.18637/jss.v095.i01.

Zhang, S., Dong, Q., Zhang, L., Xiong, Y., Liu, X., Zhu, S., 2015. Effects of water washing and torrefaction pretreatments on rice husk pyrolysis by microwave heating. Bioresour. Technol. 193, 442–448. https://doi.org/10.1016/J.BIORTECH.2015.06.142.

Zhang, S., Dong, Q., Zhang, L., Xiong, Y., 2016. Effects of water washing and torrefaction on the pyrolysis behavior and kinetics of rice husk through TGA and Py-GC/MS. Bioresour. Technol. 199, 352–361. https://doi.org/10.1016/j.biortech.2015.08.110.

Zhang, R., Zhang, J., Guo, W., Wu, Z., Wang, Z., Yang, B., 2021. Effect of torrefaction pretreatment on biomass chemical looping gasification (BCLG) characteristics: gaseous products distribution and kinetic analysis. Energy Convers. Manag. 237 https://doi.org/10.1016/J.ENCONMAN.2021.114100.